

2025
8

✓

NATIONAL ADVISORY COMMITTEE FOR AERONAUTICS

TECHNICAL MEMORANDUM

No. 1149

JUL 3 1947

THREE-COMPONENT FORCE AND MASS-FLOW MEASUREMENTS ON A JET NACELLE

By G. Ilgmann and E. Möller

Translation

"Dreikomponenten- und Durchflussmessungen an einer Strahlgondel"

Aerodynamisches Institut der Technischen Hochschule Braunschweig
Bericht Nr. 45/3



Washington

June 1947

NATIONAL ADVISORY COMMITTEE
LANGLEY MEMORIAL AERONAUTICAL
LABORATORY
Langley Field, Va.



NATIONAL ADVISORY COMMITTEE FOR AERONAUTICS

TECHNICAL MEMORANDUM NO. 1149

THREE-COMPONENT FORCE AND MASS-FLOW MEASUREMENTS
ON A JET NACELLE*

By G. Ilgmann and E. Möller

Abstract: The present report contains three-component force and mass-flow measurements on a jet nacelle at small inlet-velocity ratios $v_A/v_0 < 1$. The mass-flow measurement on two cross sections of the nacelle demonstrates the local-velocity distribution with varying flow and angle of attack.

Outline:

- I. Introduction
- II(a). Model specifications
- II(b). Symbols
- III. Test procedure
- IV. Test evaluation
- V. Test results
- VI. Summary
- VII. Bibliography

I. INTRODUCTION

The experimental investigation of jet-propulsion units, especially their performance in conjunction with the airframe, has gained great importance recently. Numerous contributions in this field have already been made by the institutes for research. Industry also shows its interest in this problem by many tests of its own. According to the report (1) measurements of the complete model are generally not necessary for a judgment of the interference effect of these propulsion units; measurements on a jet nacelle alone or on wing-nacelle configurations are sufficient.

Such a propulsion unit at small velocity ratio $v_A/v_0 < 1$ shall be investigated in the present treatise. Systematic

*"Dreikomponenten- und Durchflussmessungen an einer Strahlgondel." Aerodynamisches Institut der Technischen Hochschule Braunschweig. Bericht nr. 45/3. Braunschweig, March 8, 1945.

measurements on wing-jet nacelle configurations will follow later. It is intended to use the large amount of material on wing-fuselage configurations compiled at the Aerodynamic Institute of the Technischen Hochschule Braunschweig for estimates of the influence of jet nacelles.

Hence the first problem will be to perform three-component force measurements on a jet nacelle with flow passing through it. These measurements aim at determining the mode of dependency of the aerodynamic coefficients on the velocity ratio $\lambda = v_A/v_0$. Besides flow measurements in various cross sections shall allow insight into the velocity distribution.

II(a). MODEL SPECIFICATIONS

A jet-nacelle model of circular cross section was manufactured for this test. The model consists of a cylindrical cowling with internal spinner. Only velocity ratios $0 < \lambda < 1$ could be investigated since no blower had been built in.

The cowling inlet was selected according to Dr. Küchemann's specifications (2) for annular cowlings of type II with the constriction $F_E/F_{sp} = 0.3$, F_E representing the inlet cross section (table 1).

The tail portion of the nacelle was shaped according to the AVA-drawing No. 100 tail portion II.

The following dimensions resulted (fig. 1):

Diameter $D_{sp} = 150$ millimeters

Maximum length of the cowling $L = 750$ millimeters

Maximum length of the nacelle ($\lambda = 0$) $L_{max} = 900$ millimeters

Fineness ratio $L/D_{sp} = 5$

The mass flow was regulated solely by variation of the exit cross section. For this purpose the position of the tail portion of the spinner can be adjusted. The free-stream cross section at the exit can thus be varied in five steps, with the free cross-section areas differing by constant amounts.

The nacelle is provided with static orifices and pitot tubes (fig. 1) at sections A and B for the mass-flow measurements.

Orifices in the wall are used for determination of the static pressure. The total pressure in the slot is measured by means of a pitot tube which is radially movable. The pitot tube was made from a brass tube of the outside diameter = 1 millimeter, and the inside diameter = 0.5 millimeter. The nose of the pitot tube lies 5 millimeters ahead of the radial static orifices in the cowling. The adjustment is performed by means of a knurled nut (M 3). The pitch of the thread is 0.5 millimeter so that two revolutions cause an advance movement of 1 millimeter.

A cap was put over the opening for the incoming flow for the measurement of the jet nacelle as a streamline body. The dimensions are shown in figure 1. The small step at the tail between cowling and spinner of the nacelle (in throttle position 4) was not filled out with clay for the measurement of the streamline body.

II(b). SYMBOLS

The sense of direction of forces and moments is established according to DIN L 100, 2. edition. The symbols used are enumerated below:

D_{sp}	maximum diameter of the nacelle
F_{sp}	largest bulkhead area of the nacelle ($F_{sp} = 0.0177 \text{ m}^2$)
L	length of the nacelle (cowling)
L'	length of the nacelle (with streamlined tail portion)
F_R/F_{sp}	contraction of the cowling inlet
F_A	exit cross section (0.00535 m^2)
$R_{cowling}$	inner radius of the cowling at the cross sections of measurements A and B
$R_{spinner}$	outer radius of the spinner at the cross sections of measurements A and B
λ	velocity ratio (v_A/v_0)
v_0	undisturbed velocity of the incident flow (m/s)

v_A	mean velocity at the exit cross section (m/s)
Q	mass flow (m^3/s)
α	angle of attack
q	dynamic pressure of the undisturbed flow $\left(\frac{\rho}{2} v_o^2\right)$
c_a	lift coefficient of the nacelle $\left(\frac{A}{q F_{sp}}\right)$
c_w	drag coefficient of the nacelle $\left(\frac{W}{q F_{sp}}\right)$
c_M	moment coefficient with respect to the lateral axis; point of reference: axis of the nacelle at the inlet cross section $\left(\frac{M}{q F_{sp} L}\right)$
λ	friction coefficient of the tube $\left(\frac{p}{\frac{\rho}{2} \bar{v}^2} \frac{d}{l}\right)$
l	distance of the cross sections of measurements A and B ($l = 200$ mm)

III. TEST PROCEDURE

The measurement was carried out in the 1.2-meter wind tunnel of the AITHB at a wind velocity of $v_0 = 40$ m/s. The velocity ratio was varied within the limits $0 < \lambda < 0.76$.

The three-component force measurement was to give information on the aerodynamic quantities of the jet nacelle for various throttlings of the mass flow. For comparison the nacelle was measured with a streamlined bowling. Moreover, two variations of the nacelle were investigated at $\lambda = 0$: (a) nacelle with nose cap and without tail cone; (b) nacelle without nose cap and without tail cone. (See fig. 2, configurations 7 and 8.)

A wake survey was used to determine the wire drag of the model suspension.

The measurement of the pressure distribution in the cross sections of measurements A and B (fig. 1) led to the determination of the mass flow and of the velocity distribution. The velocity distribution and the mass flow in the exit cross section at an angle of attack $\alpha = 0^\circ$ were ascertained for control.

The test program is given in table 2.

IV. TEST EVALUATION

(a) Force Measurement

The results of the three-component measurement are represented nondimensional:

$$C_a = \frac{A}{q F_{sp}} ; \quad C_w = \frac{W}{q F_{sp}} ; \quad C_M = \frac{M}{q F_{sp} L}$$

The selected reference values were:

$$F_{sp} = 0.0167 \text{ m}^2 = \text{largest bulkhead area}$$

$$L = 0.750 \text{ m} = \text{length of the nacelle}$$

The point of reference for the longitudinal moment lies at midaxis of the nacelle inlet area.

The wire drag of the model support which was ascertained by wake survey was subtracted accordingly. The wire drag for these measurements lies between the limits $w_{nacelle}/w_{suspension} = 0.25$ to 0.40.

The Reynolds number for the three-component-measurement is $vL/\nu = 2.0 \times 10^6$, referred to the length of the nacelle $L = 750$ millimeters.

(b) Mass-Flow Measurements

First, the local velocity distribution in the slot between spinner and cowl can be ascertained from the measured distribution of total pressure and static pressure. The value of the mass flow follows by integration:

$$Q = 2\pi \int_{r=R_{hub}}^{r=R_{cowl}} v(r) r \, dr$$

The mean mass-flow results from the comparison of the four test points in the cross section of measurements. From this figure the mean velocity at the exit cross section can be calculated with which the velocity ratio λ is formed. The measurements taken for comparison at the sections A and B and at the exit cross section permit an estimate of the accuracy of the method of measurement. (See table 3.)

Values of the mass flow Q (m^3/s)

Therewith results a maximum deviation from the mean mass flow of 1.5 percent. The measurement of velocity distribution near the wall is generally very sensitive due to the large velocity gradient.

The static pressures which were ascertained for the sections A and B make a comparison to the known friction coefficients of the tube possible.

V. TEST RESULTS

The separate results of the force measurement are represented in the figures 3 to 10. The $c_a(\alpha)$ -, $c_p(\alpha)$ -curves and the polars for the most important cases are summarized in figures 11 and 12.

Figure 13 shows the drag coefficients c_{w0} of the nacelle for $\alpha = 0^\circ$ and various amounts of air passing through. A few measurement values from an AVA-report (3) are drawn in for comparison. The drag of the test nacelle at $\lambda \sim 0.6$ is higher than the comparative value of the AVA-measurement and higher than the customarily given value $c_{w0} = 0.10$ to 0.12 (1). The test points intimate a drag increase with increasing throttling.

The contribution of the inside drag can be seen from a comparison of the nacelle drags with and without flow passing through. This contribution can be traced back to the drag of the spinner and to the friction drag on the inside of the cowlings. The difference $\Delta c_w = c_w(\text{mass flow}) - c_w(\lambda = 0) \sim 0.05$ also is larger than in the AVA measurement mentioned above.

The jet nacelle with a streamlined cowlings produces only a small drag reduction. In the variations additionally measured (figs. 9 and 10) the unfavorable influence of the missing tail

cone is shown by a drag increase. The unfavorable tail configuration of the ellipsoid of revolution $1:7^1$ has the same effect.

The compilation in chart 14 elucidates the relations with respect to lift and pitching moment; dc_a/da , dc_m/da , and dc_{m1}/dc_a are represented there as functions of λ and compared with existent test results. Two ranges of $\alpha = -6^\circ$ to 6° and $\alpha > 6^\circ$, with essentially differing increases, result for the lift increase dc_a/da . The lift increase with λ can be seen clearly.

The change in moment increase dc_m/da (moment reference point to axis of the nacelle at the inlet cross section) for the measured nacelle in the range $0 < \lambda < 0.76$ is small. One can recognize, however, that the unstable moment of the nacelle somewhat decreases with the mass flow. The moment curves (fig. 11) also show that for this cowl separation starts between $\alpha = 6^\circ$ to 9° .

Concerning the problem of the neutral point it is more favorable, according to Multhopp, to have determined the neutral point for the friction lift. For this case solely the moments which are caused by lift forces are considered. The free moment as it is obtained under the assumption of frictionless flow without resulting forces on the body of the nacelle, is subtracted from the measured moment. According to Munk (see (4)) the free moment can be ascertained for slender bodies:

$$\frac{1}{q} \frac{dM}{da} = 2 \text{ Vol } (k_2 - k_1)$$

$(k_2 - k_1)$ is a correction term for the fineness ratio.

The correction factor can be applied approximately to the jet nacelle. As a result, figure 15 shows the position of the neutral point of the existent friction lift as a function of a form factor

$f = \frac{2}{\pi q D_{sp}^2} \frac{dA}{da}$ which is dependent on the special lift relations of the nacelle. A definite lawfulness in the position of the neutral

¹Test body for wing-fuselage combinations measured at the Aerodynamic Institute of the Technischen Hochschule Braunschweig, see: Möller, "Systematische Sechskomponenten-Messung an Flügel-Rumpf-Anordnungen. Jahrbuch der Deutschen Luftfahrtforschung 1942, I., p. 336.

point of the friction lift can be seen. With the form factors being equal the neutral point lies considerably further back for the nacelle than for slender bodies. The position of the neutral point of the friction lift for the ellipsoid of revolution 1:7 which was graphically represented for comparison approaches more the one for slender bodies (5).

According to IV(b) one first determines from the measurement of pressure distribution the dependency of the mass flow on the throttle position. A survey is given in figure 16. The highest velocity ratio obtained for this configuration is $\lambda = 0.76$.

Taking the measured static pressures within the nacelle into consideration one can use the pressure measurement for determination of the tube friction coefficient λ_{tube} . The hydraulic radius $r' = F/U$ must be substituted for d in the well known formula

$$\lambda_{\text{tube}} = \frac{\Delta p}{\frac{\rho}{2} \bar{v}^2} \frac{d}{l}$$

(F = cross-sectional area of mass flow, U = wetted circumference); therefore

$$\lambda'_{\text{tube}} = \frac{\Delta p}{\frac{\rho}{2} \bar{v}^2} \frac{r'_h}{l}$$

with $\bar{v} = Q/F$ = mean flow velocity at the cross section of measurements, l = distance between the two pressure test points and r'_h the hydraulic radius, = 0.0085 meter. It is noteworthy that with the substitution of the hydraulic radius

λ'_{tube} becomes $1/4 \lambda_{\text{tube}}$ and $Re'_e = \frac{\bar{v} r'_h}{\nu} = \frac{Re}{4}$. The

interior of the jet nacelle is well polished and the nacelle can therefore be regarded as a smooth tube. Nevertheless the values valid for smooth tubes are not reached (fig. 17) for the reason that the flow is in starting condition. (See fig. 20, section A and B.) Figures 18 and 19 show the influence of the angle of attack upon the flow conditions for the jet nacelle. A comparison of the four test points in the cross section of measurements A (fig. 18) shows up to $\alpha = 12^\circ$ a good agreement in the velocity distribution. Only at $\alpha = 18^\circ$ a flow displacement can be noticed at test point 1; this

displacement is clearly discernible for both throttle positions. Figure 19 shows the same tendency for test point 1. However, this one-side flow displacement does not influence the mass flow.

Due to the rapid increase in velocity near the wall, a slight dispersion of the test points is unavoidable in this range; therefore they lie within the accuracy of measurement of the test method used. The differences in velocity at the center of the cross section of measurements at $\alpha = 0^\circ$ (fig. 18) are caused by a slightly off center position of the spinner. Figure 19 shows for all test points a small increase of the flow velocity with increasing angle of attack. This phenomenon is most probably caused by the influence of the domain of underpressure increased with increasing angle of attack at the tail of the nacelle.

VI. SUMMARY

Force and mass-flow measurements were carried out on a jet nacelle with the velocity ratio $0 < v_A/v_0 < 0.76$. The result of the three-component force measurement is an increase of the lift curve slope and a decrease of the unstable moment of the nacelle with mass flow. The neutral point of the friction lift which lies at $x_N/L = -0.93$ for $\lambda = 0$ travels forward with increasing mass flow. The mass-flow measurement elucidates the flow behaviour in the inner space of the nacelle. An even velocity distribution in the annular cross section is to be found up to an angle of attack of 12° . The one-side flow displacement which appears at $\alpha = 18^\circ$ exercises no influence upon the mass flow.

Translated by Mary L. Mahler
National Advisory Committee
for Aeronautics

VII. BIBLIOGRAPHY

1. Schlichting, H.: Untersuchungen über den Einbau von Gondelkörpern. UM 2094, 1944.
2. Küchemann, D., and Weber, J.: Das Einlaufproblem bei Triebwerksverkleidungen. Mitteilungen der Deutschen Akademie der Luftfahrtforschung 1943.
3. Bäuerle/Weber: Der Anbau von T.L.-Triebwerken an den Tragflügeln, 1. Teilbericht: Kraft- und Druckverteilungsmessungen an Triebwerksgondeln (UM. 3147) 1944.
4. Multhopp F.: Aerodynamics of the Fuselage, NACA TM No. 1036, Dec. 1942.
5. Lochmann, L.: Druckverteilungsmessungen an einem Mitteldecker bei symmetrischer Anströmung. FB 1710/2, 1943.

TABLE 1

COORDINATES OF THE COWLING INLET ACCORDING TO KÜCHEMANN/WEBER (2)

$F_E/F_{sp} = 0.30$		$(F_E = \text{Inlet cross section})$	
(1) Coordinates of the outside		(2) Coordinates of the inside	
$x/R_E =$	$r/R_E =$	$x/R_E =$	$r/R_E =$
0	1.237	0	1.237
.05	1.370	.05	1.113
.1	1.426	.1	1.075
.2	1.500	.15	1.056
.3	1.553	.2	1.035
.4	1.596	.3	1.015
.5	1.633	.4	1.005
.6	1.665	.5	1.001
.7	1.693	.6	1.000
.8	1.718		
.9	1.740		
1.0	1.759	(3) Radius of curvature ρ/R_E	
1.1	1.774	(Coordinates of the center of curvature:	
1.2	1.787	$x = \rho; \quad r = r(x = 0)$	
1.3	1.798	$\rho/R_E = 0.175$	
1.4	1.807		
1.5	1.815		
1.6	1.821		
1.7	1.825		
1.8	1.826		
1.9	1.826		
2.0	1.826		

TABLE 2
TEST PROGRAM

Program item	Dynamic pressure q (kg/m ²)	Angle of attack α°	Throttle position	$\lambda = v_A/v_o$	Figure no.
(a) Three-component measurement					
1	100	$\alpha^\circ = -6; -3; 0$	0	0.76	3
2	100	3, 6, 9	2	.63	4
3	100	12, 15	3	.49	5
4	100	18, 21	4	0	6
5	100	$\alpha^\circ = -6; -3; 0$	Streamline body	0	7
6	100	3, 6, 9, 12, 15	Variation: Jet nacelle without tail cone	0	9
7	100	18, 21	Variation: Streamline body without tail cone	0	10

TABLE 2 - Concluded

TEST PROGRAM - Concluded

Program item	Dynamic Pressure $q \text{ (kg/m}^2\text{)}$	Angle of attack α°	Throttle position	λ	Notes	Figure no.
(b) Mass-flow measurements						
8	100	0°	0	0.76	Measurement in the section A, B and nacelle exit	20
9	100	0°	2	.63		
10	100	0°	3	.49		
11	100	$6^\circ, 12^\circ, 18^\circ$	0 ; 2	.76	Measurement in the section A	18
12	100	$6^\circ, 12^\circ, 18^\circ$	0 ; 2	.63		19

TABLE 3

COMPARISON OF THE MEAN MASS FLOWS AT THREE CROSS SECTIONS
OF MEASUREMENT

Throttle position	0	2	3
Gross section of measurements { A B	0.1612 .1617	0.1358 .1340	0.1040 .1055
Exit cross section	.1630	.1367	.1074
Mean value	.1620	.1355	.1058
Maximum deviation from the mean value in percent	.6	1.1	1.5

TABLE 4

VELOCITY RATIO $\lambda = v_A/v_0$ IN DEPENDENCY ON THE THROTTLE POSITION

Throttle position	$\frac{F_{\text{throttled}}}{F_{\text{free}}}$	$Q \text{ (m}^3/\text{s)}$	$v_A \text{ (m/s)}$	$\lambda = v_A/v_0$ ($v_0 = 40 \text{ m/s}$)
0	1	0.1620	30.3	0.76
2	.50	.1355	25.3	.63
3	.25	.1056	19.7	.49
4	0	0	0	0

TABLE 5

TUBE FRICTION COEFFICIENT AS A FUNCTION OF THROTTLING

Throttle position	$\frac{v_A}{v_0}$ ($v_0 \sim 40 \text{ m/s}$)	\bar{v} (m/s)	λ_{tube}	$Re = \frac{v d}{\nu}$
0	0.76	30.8	2.48×10^{-2}	6.92×10^4
2	.63	26.1	2.66	5.86
3	.49	20.1	3.20	4.52

scale 1:4

sketch of the jet nacelle according to drawing No. 494 of the AJTEB

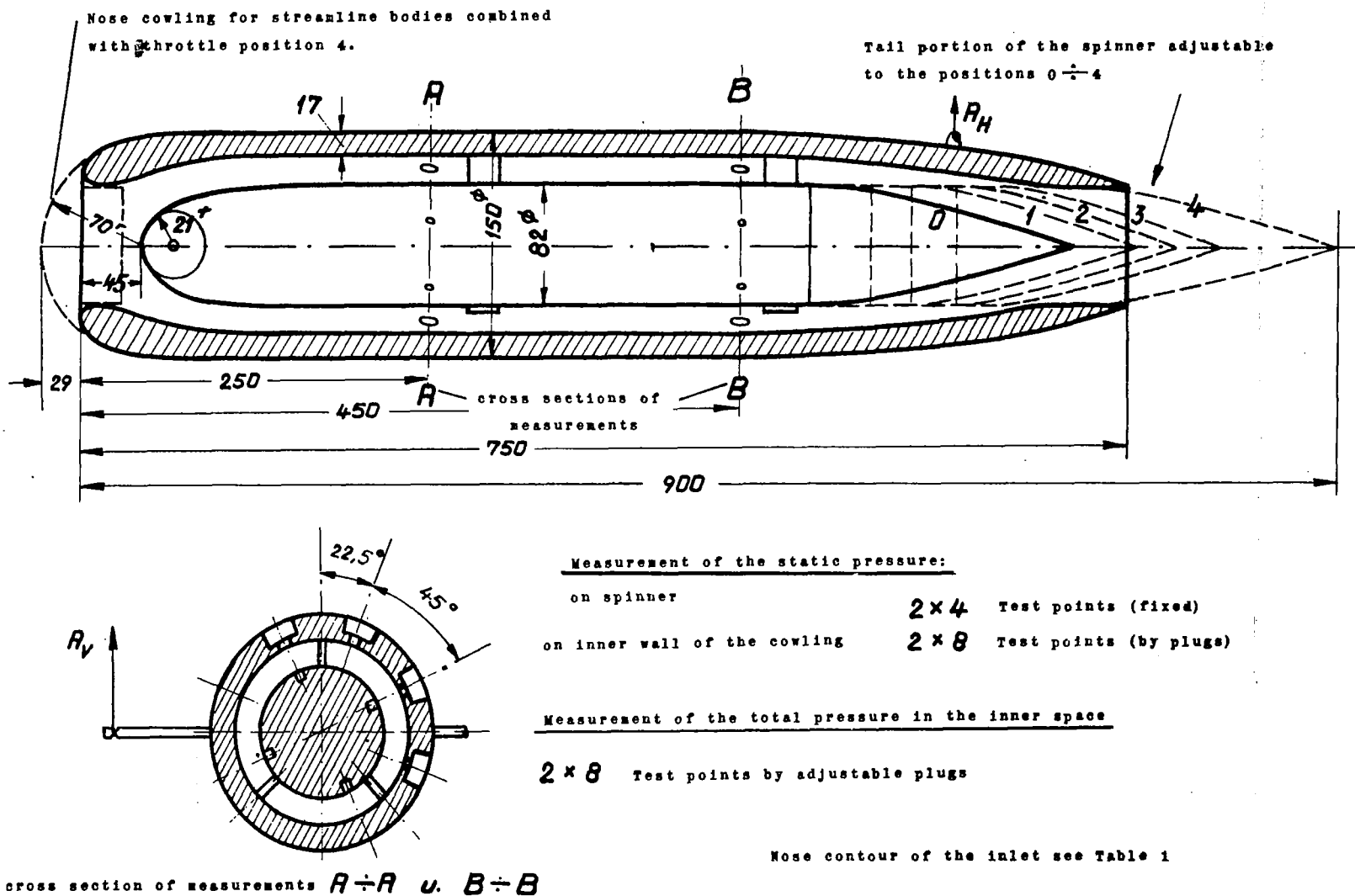


Figure 1. Survey of the model.

Fig. 2

NACA TM No. 1149

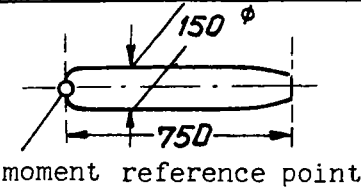
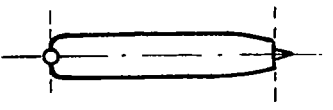
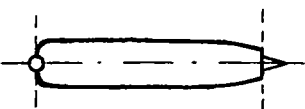
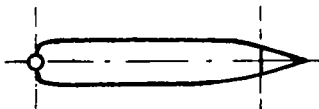
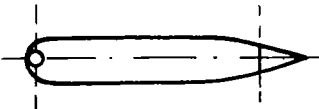

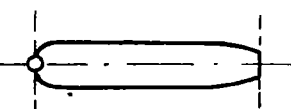
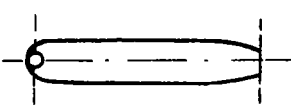
configuration	sketch	throttle position	$\frac{L}{D}$	$\lambda = \frac{V_R}{V_D}$	result in Fig.
①		0	5,0	0,76	3
②		2	5,2	0,63	4
③		3	5,4	0,49	5
④		4	6,0	0	6
⑤		stream-line body	6,1	0	7
⑥		ellipsoiol of revolution 1:7	7,0	0	8
⑦		jet nacelle without tail cone	5,0	0	9
⑧		streamline body without tail cone	5,2	0	10

Figure 2. Test program of the three-component force-measurement (survey).

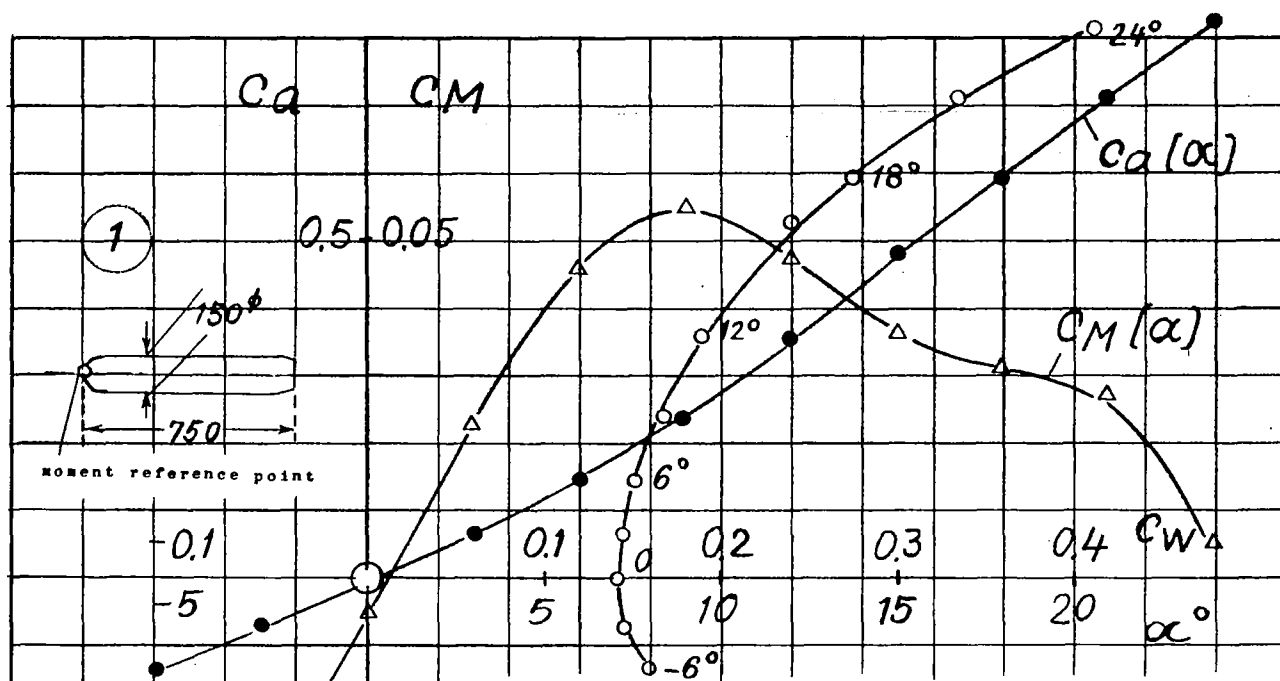


Figure 3. Jet nacelle $\lambda = V_A - V_0 = 0.76$ three-component force measurements $C_L(\alpha)$; $C_D(\alpha)$; $C_M(\alpha)$.

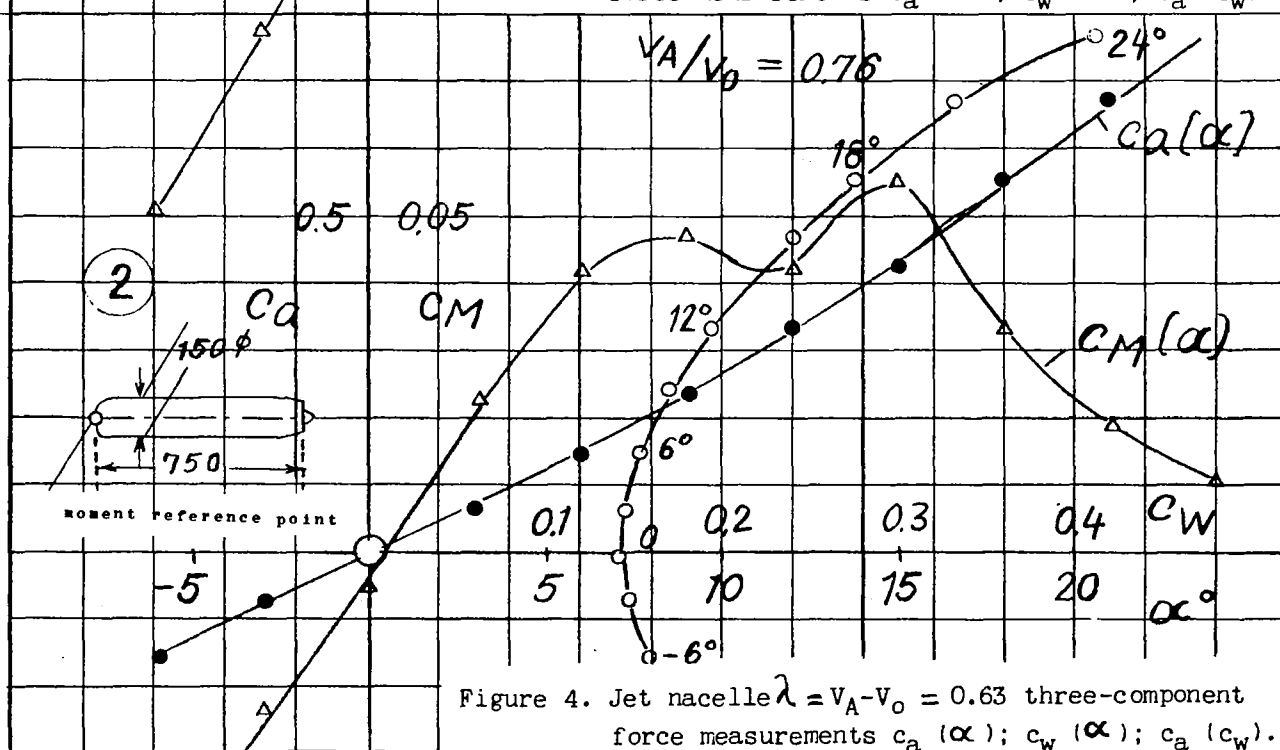


Figure 4. Jet nacelle $\lambda = V_A - V_0 = 0.63$ three-component force measurements $C_L(\alpha)$; $C_D(\alpha)$; $C_M(\alpha)$.

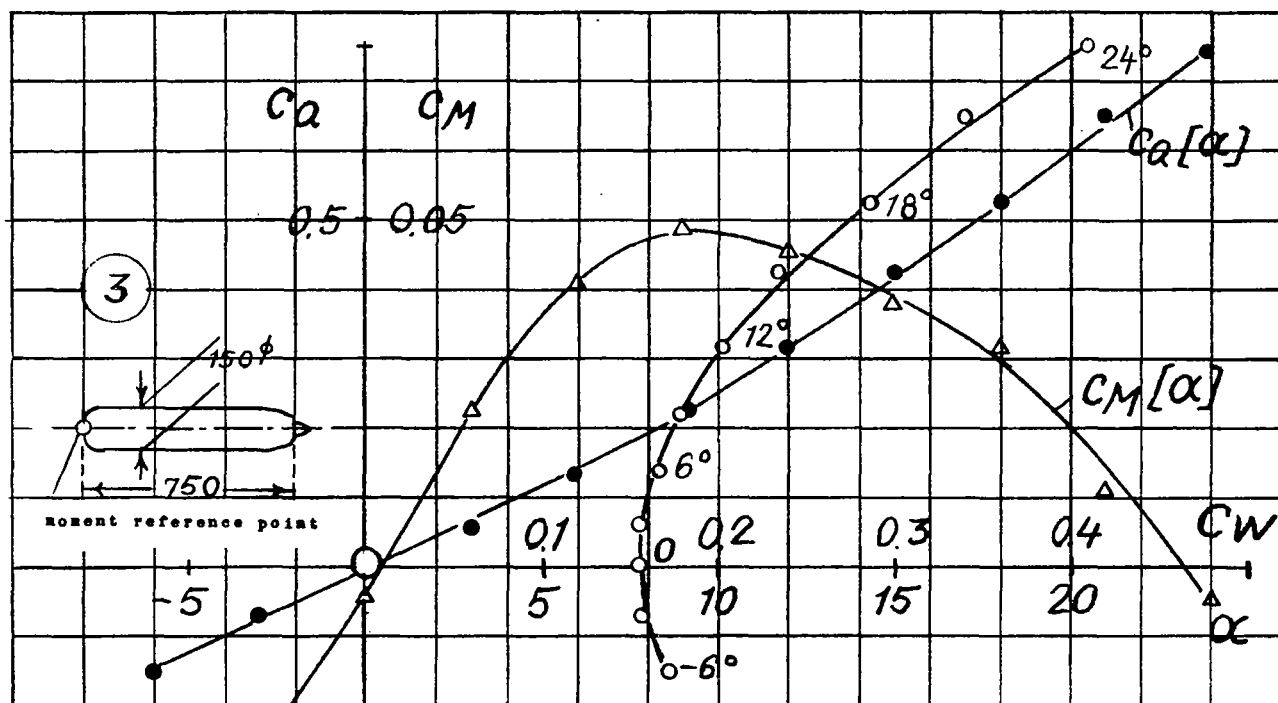


Figure 5. Jet nacelle $\lambda = V_A/V_0 = 0.49$ three-component force-measurements $c_a(\alpha)$; $c_w(\alpha)$; $c_a(c_w)$.

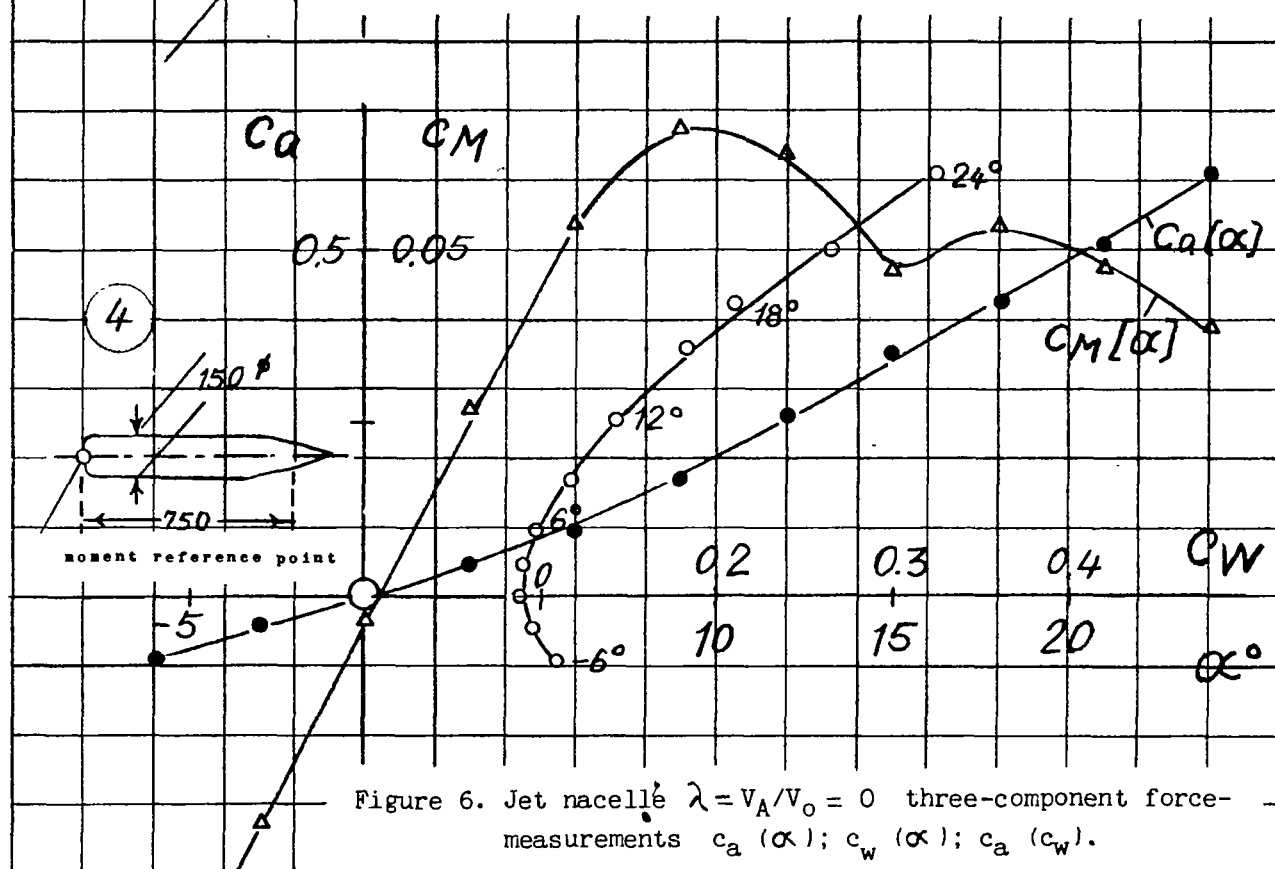


Figure 6. Jet nacelle $\lambda = V_A/V_0 = 0$ three-component force-measurements $c_a(\alpha)$; $c_w(\alpha)$; $c_a(c_w)$.

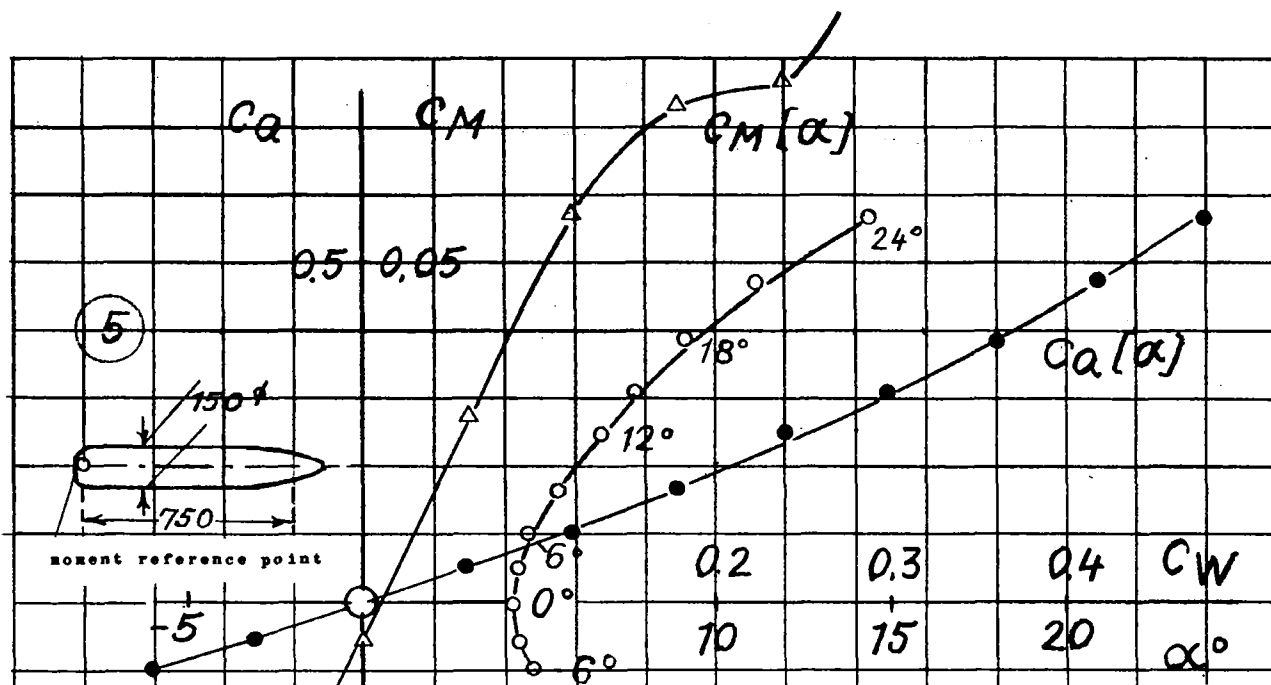


Figure 7. Streamline body; three-component force-measurements $c_a(\alpha)$; $c_w(\alpha)$; $c_a(c_w)$.

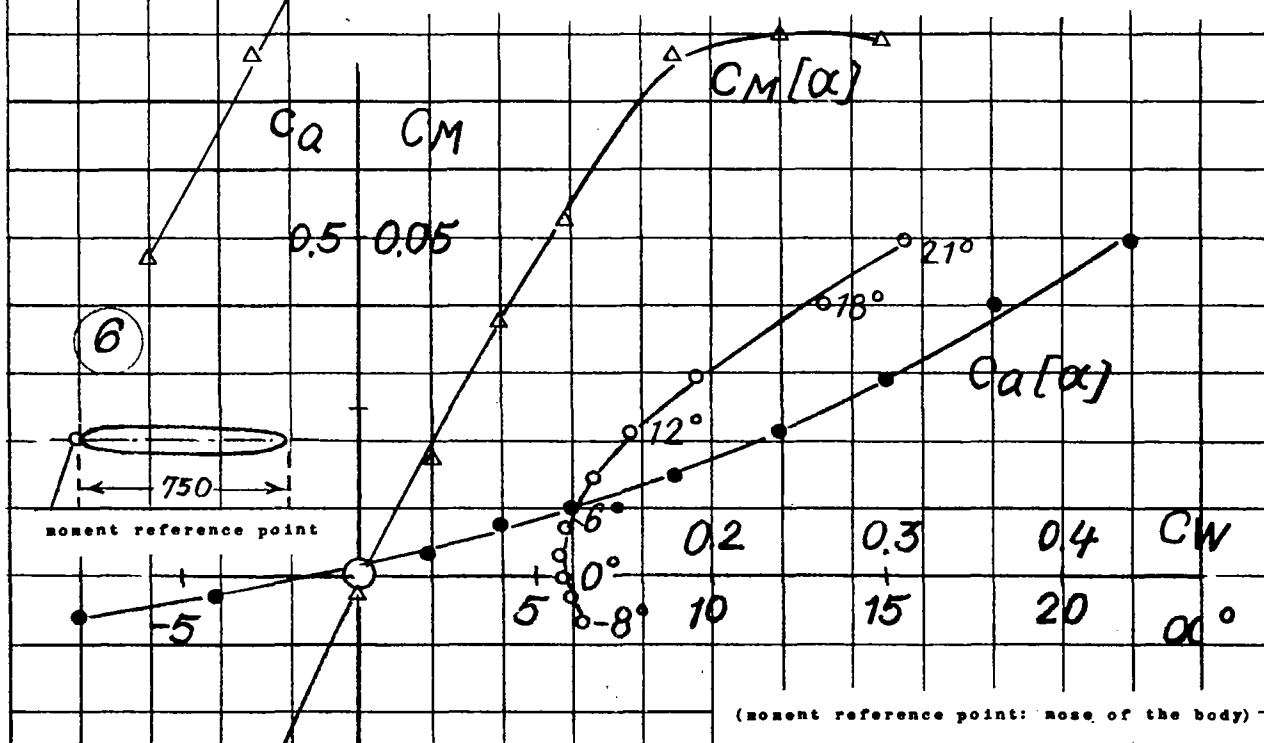


Figure 8. Ellipsoid of revolution 1:7 three-component force-measurements $c_a(\alpha)$; $c_w(\alpha)$; $c_a(c_w)$.

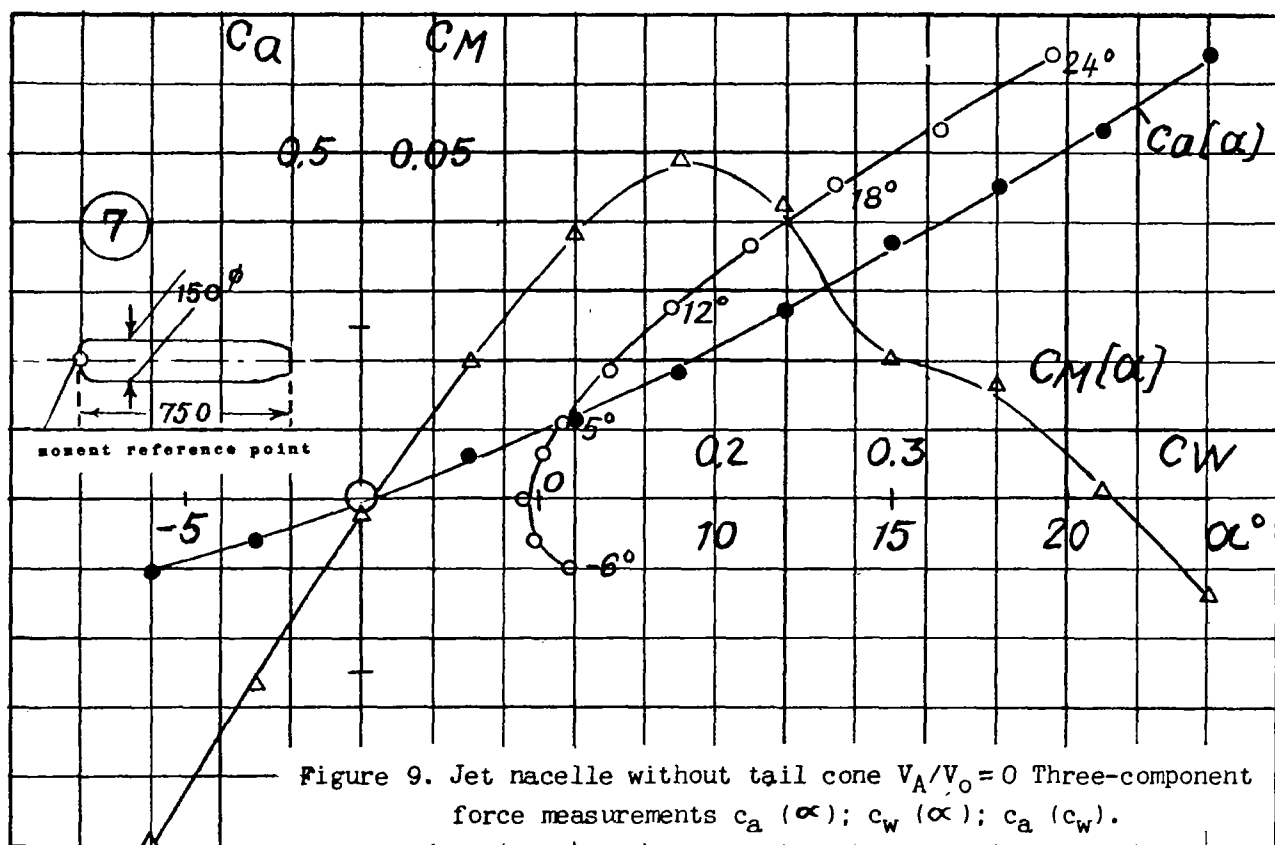


Figure 9. Jet nacelle without tail cone $V_A/V_0 = 0$ Three-component force measurements $c_a(\alpha)$; $c_w(\alpha)$; $c_a(c_w)$.

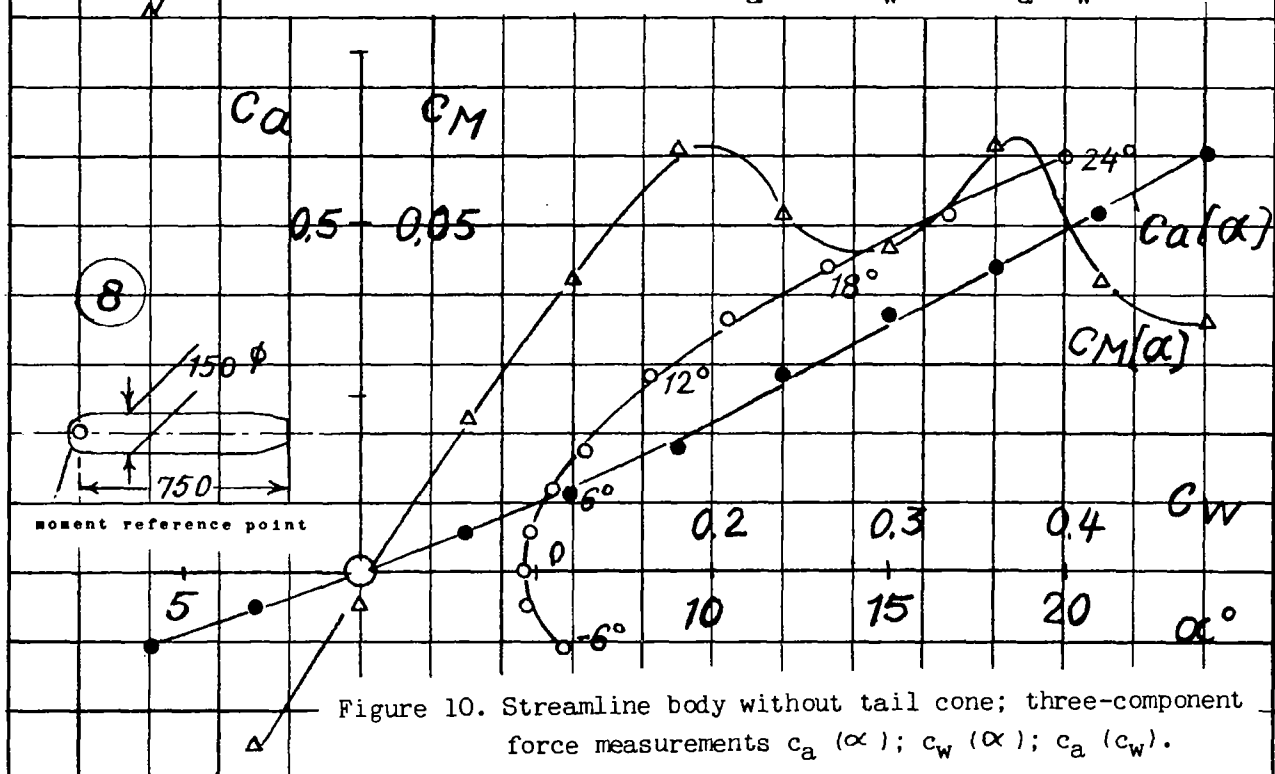


Figure 10. Streamline body without tail cone; three-component force measurements $c_a(\alpha)$; $c_w(\alpha)$; $c_a(c_w)$.

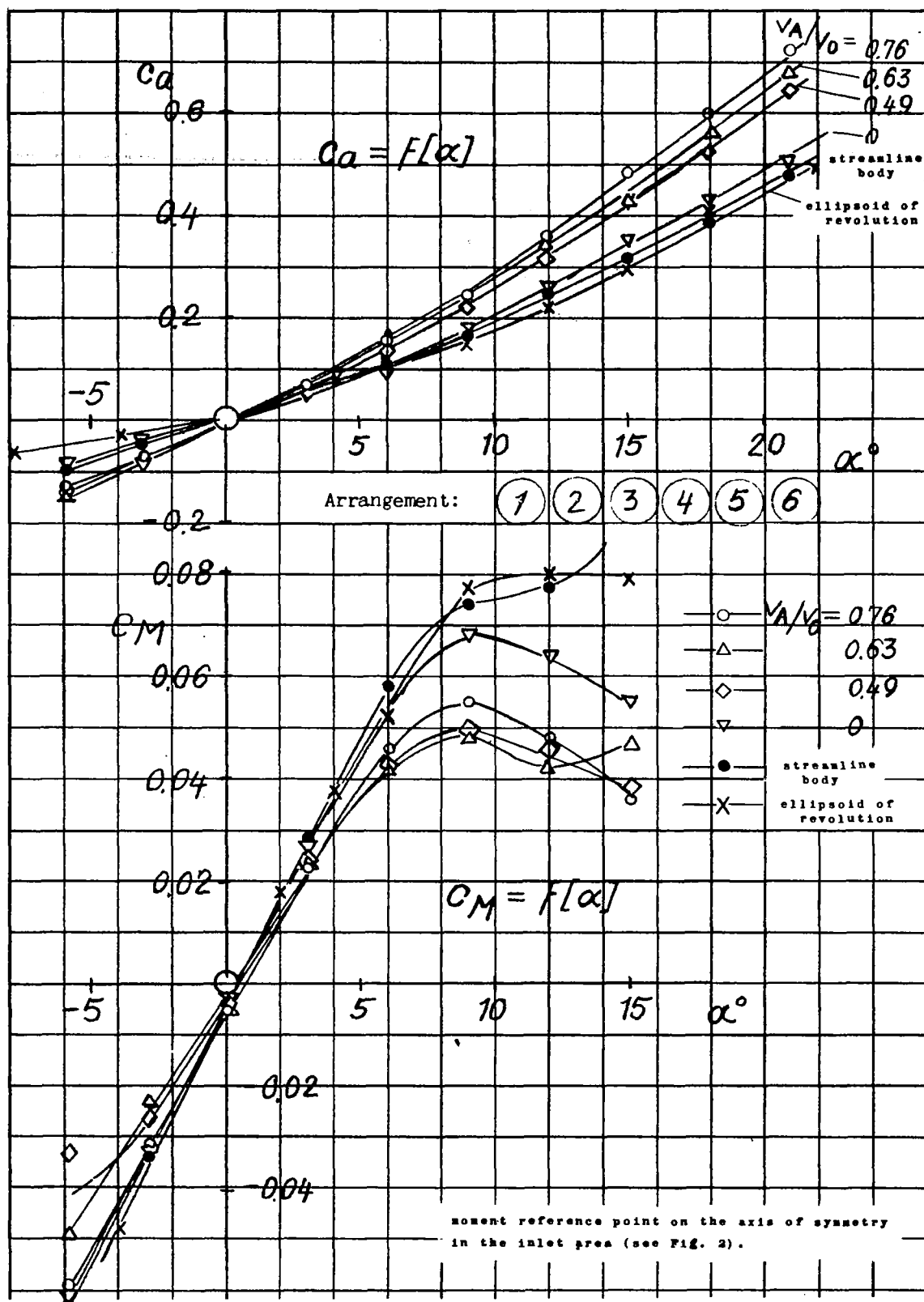


Figure 11. Joint representation of $c_a(\alpha)$ and $c_M(\alpha)$ from the separate results (Fig. 3 to 8).

Fig. 12

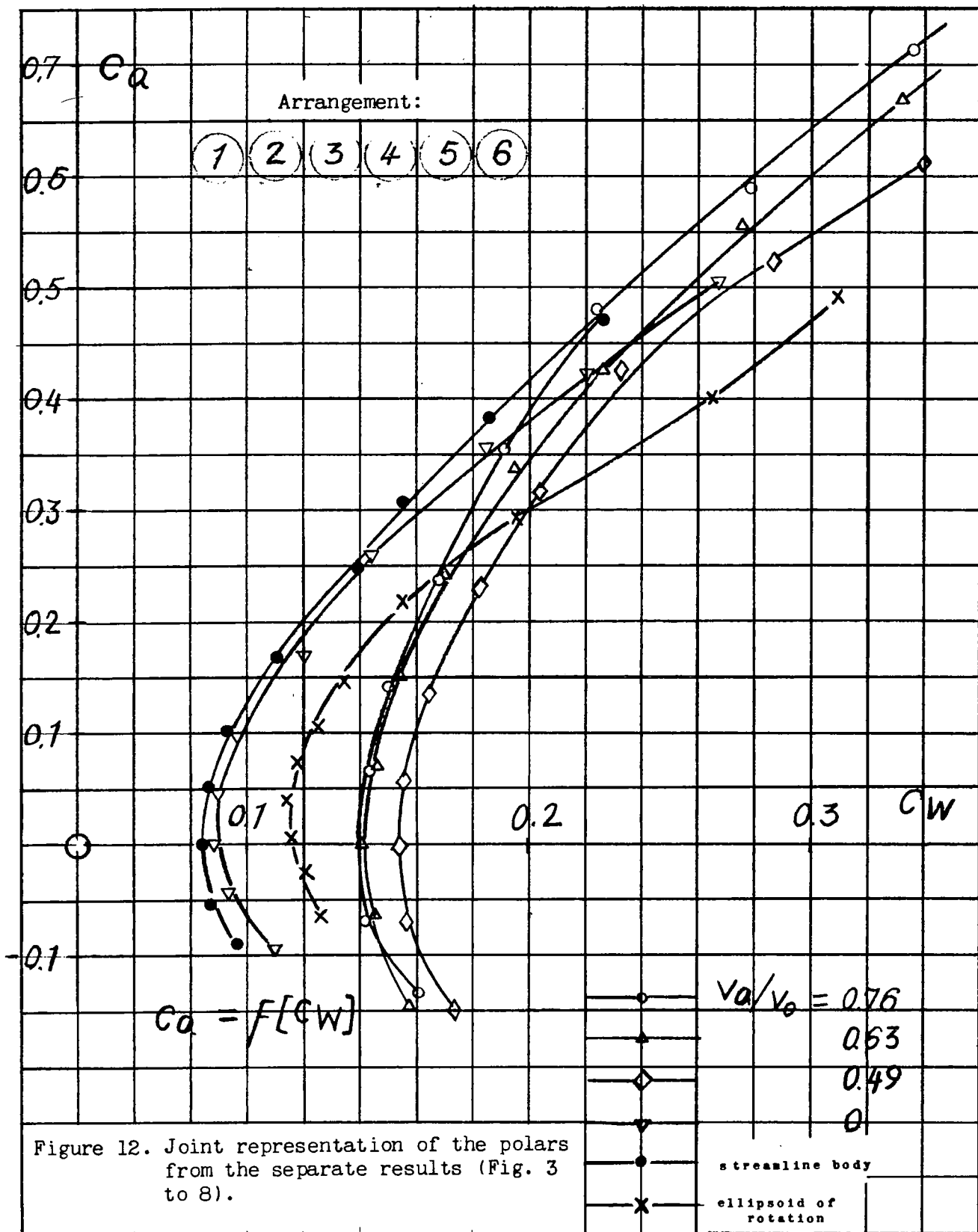
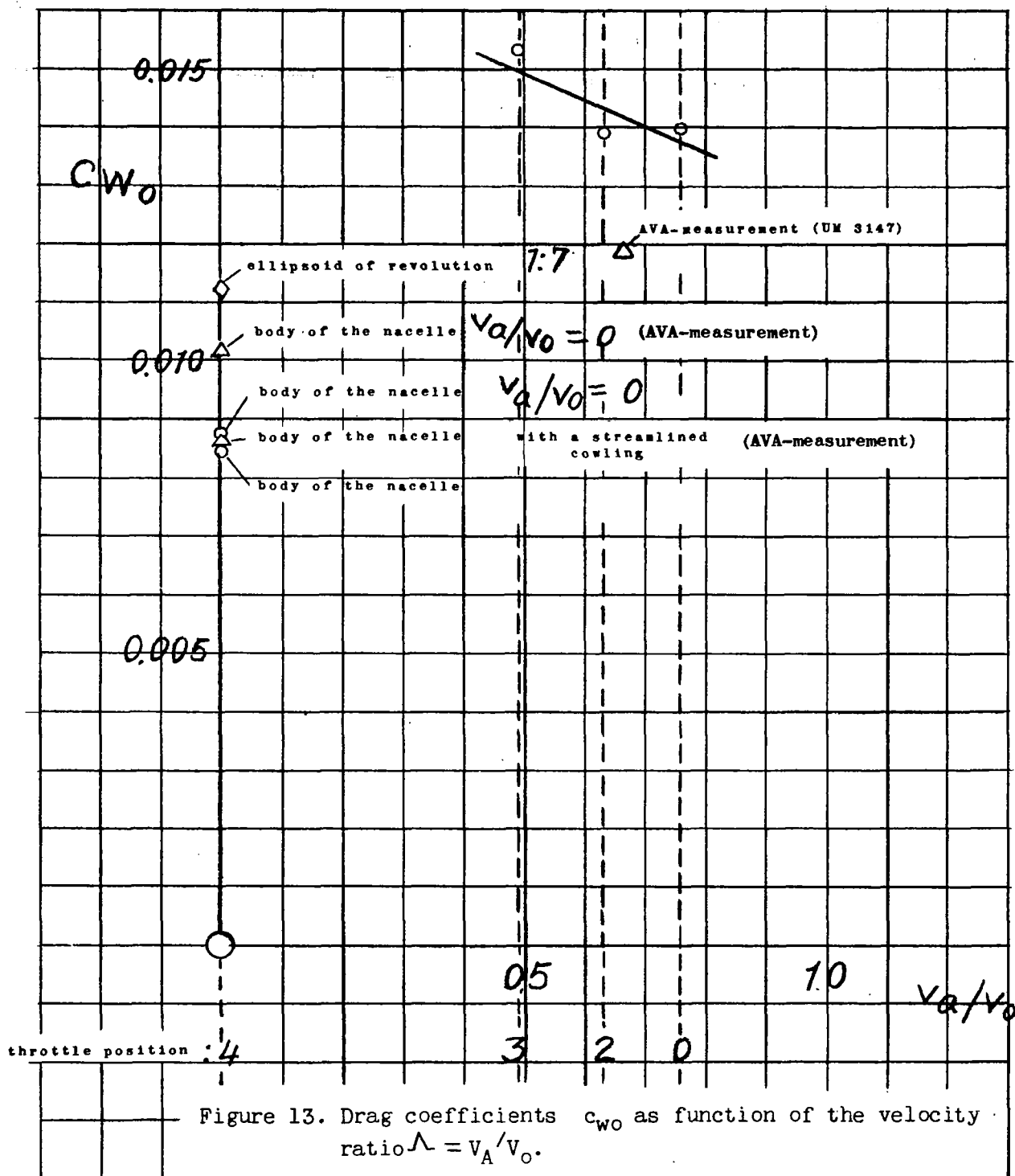
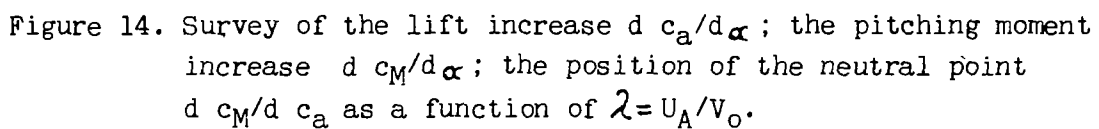


Figure 12. Joint representation of the polars from the separate results (Fig. 3 to 8).



Drag coefficients referred to largest bulkhead area



$$F = \frac{1}{\frac{\gamma C}{2} \cdot q \cdot b_R^2} \cdot \frac{dR}{d\alpha}$$

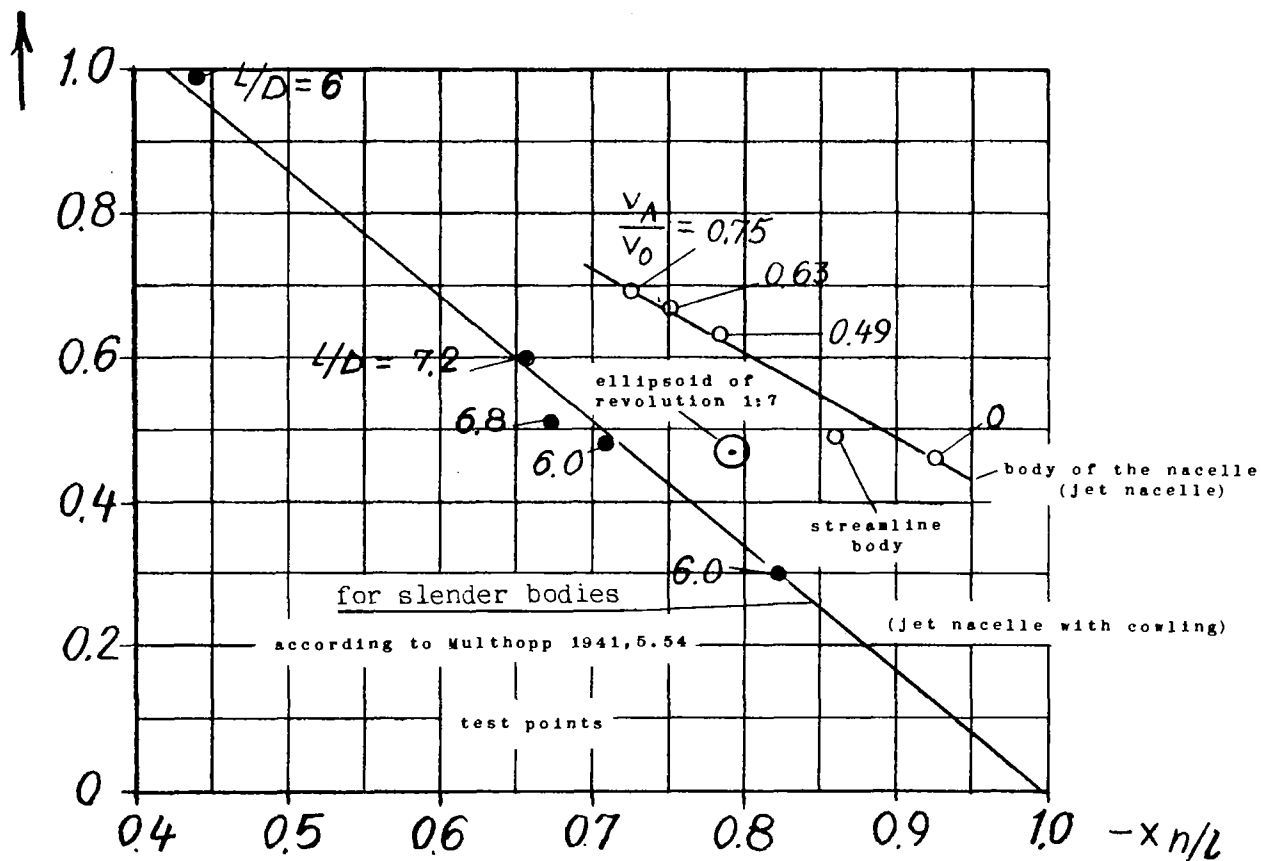


Figure 15. Position of the neutral point of the friction lift.

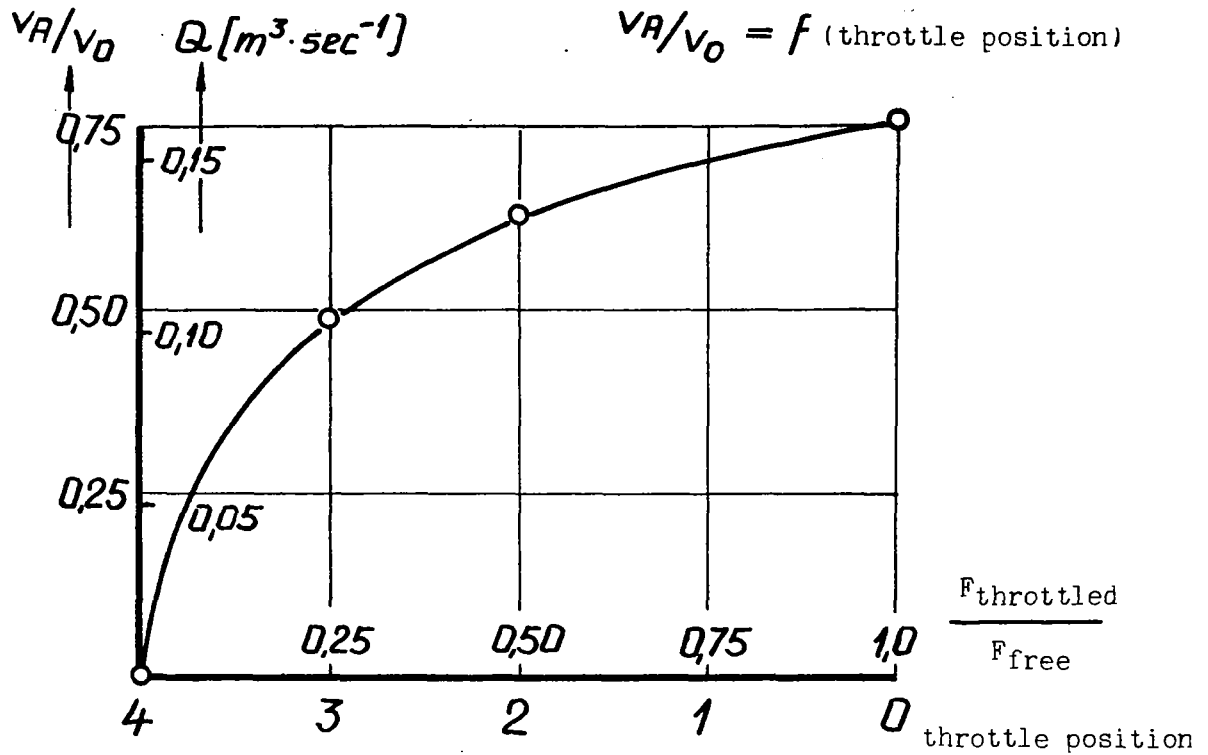
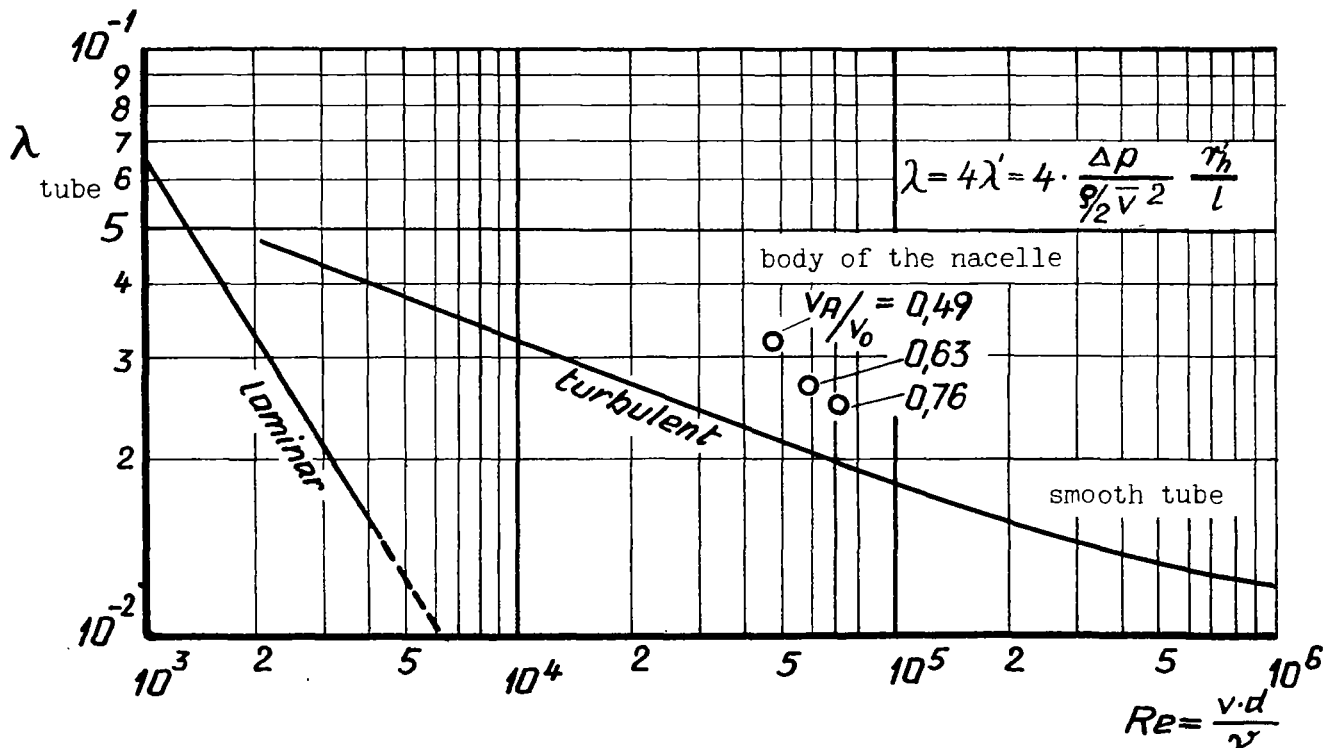


Figure 16. Velocity ratio as a function of the throttle position.

Figure 17. Comparison of the tube friction coefficients as functions of Re .

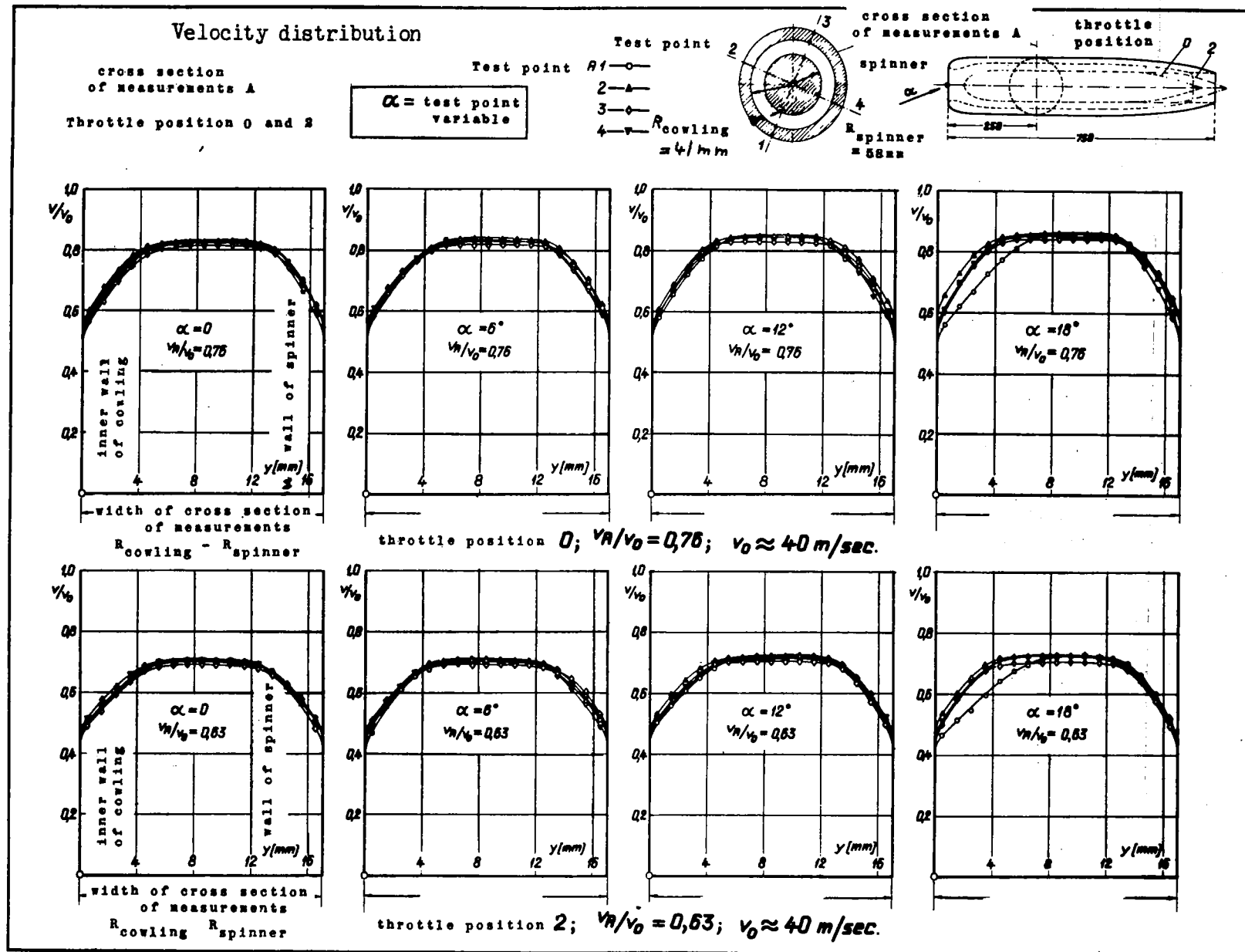


Figure 18. Velocity distribution in the cross section of measurements A $\alpha = \text{const.}$, test point variable.

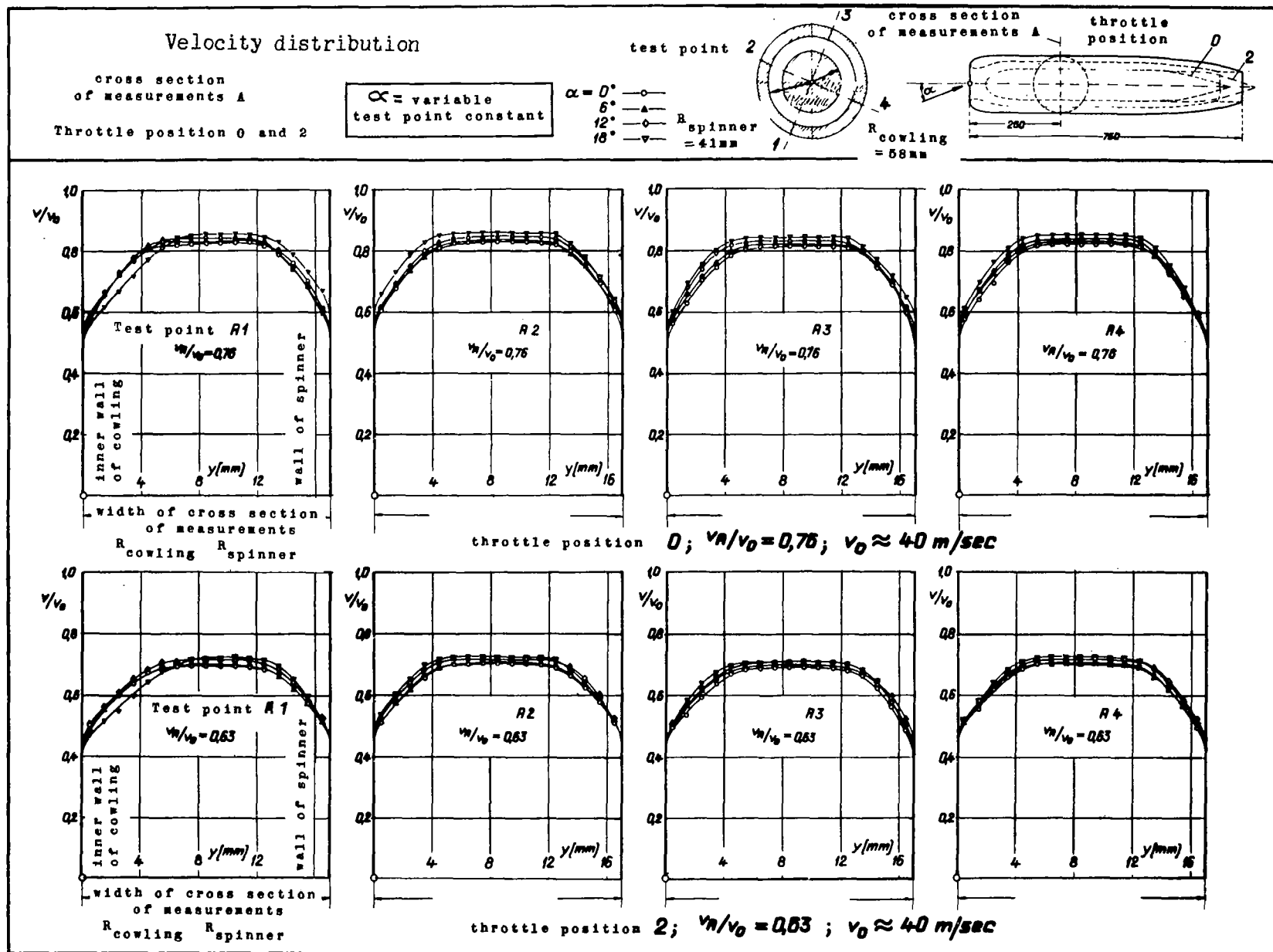


Figure 19. Velocity distribution in the cross section of measurements A $\alpha = \text{variable}$, test point constant.

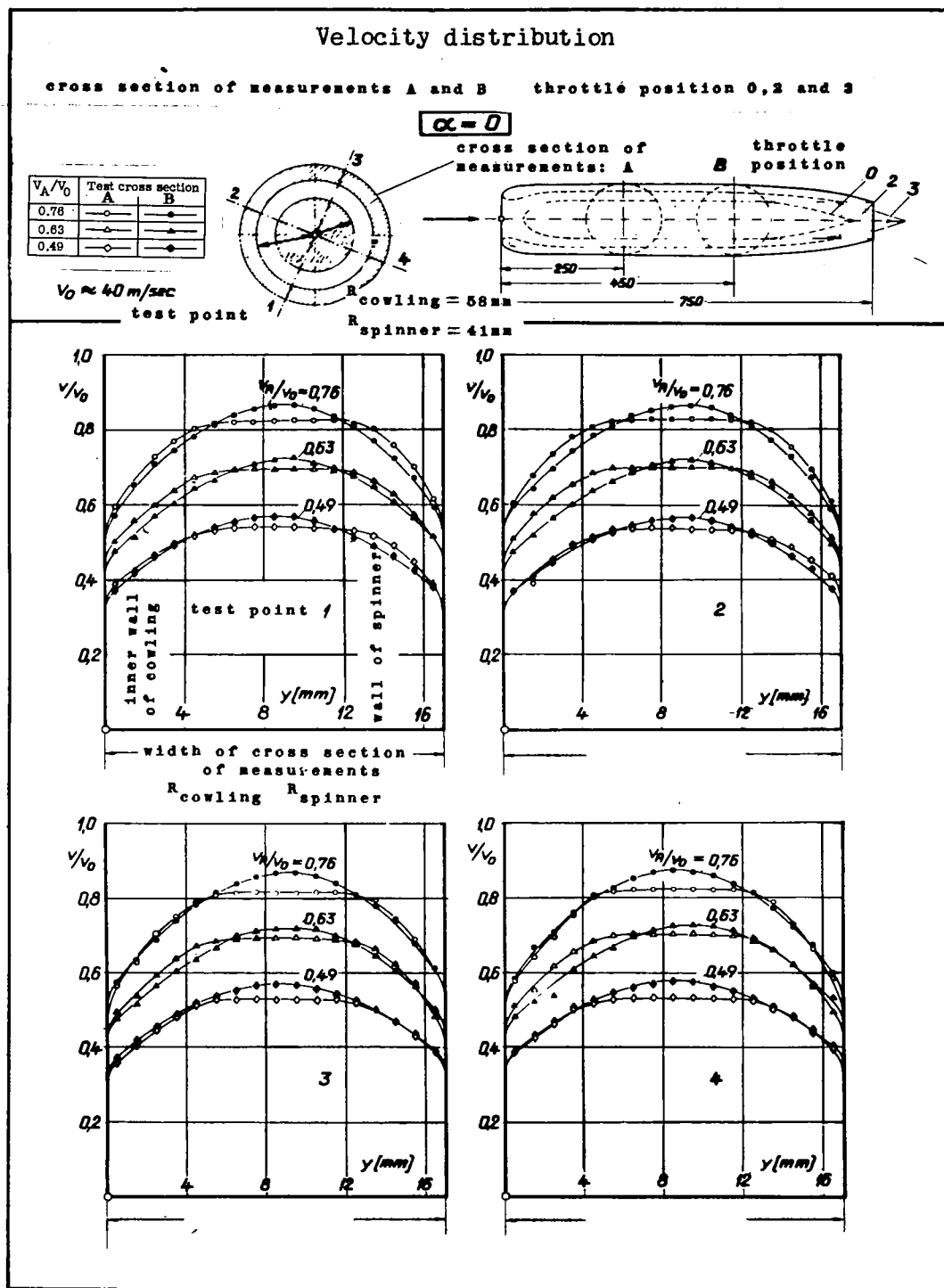


Figure 20. Velocity distribution in the cross section of measurements A and B $\alpha = \text{const.} = 0^\circ$.

NASA Technical Library



3 1176 01437 4541